DOI: 10.15669/pnst.8.86

Progress in Nuclear Science and Technology
Volume 8 (2025) pp. 86-91

ARTICLE

Validation of the TWOPORFLOW Turbulent Mixing Model with Cross-Flow Experimental Data of the MOTEL Facility

Alejandro CAMPOS-MUÑOZ*, Victor Hugo SANCHEZ-ESPINOZA and Uwe IMKE

Karlsruhe Institute of Technology, Institute of Neutron Physics and Reactor Technology, Hermann-von-Helmholtz-Platz 1, 76344, Eggenstein-Leopoldshafen, Germany

The LUT University has conducted safety-related experiments at the MOTEL facility, a representation of the NuScale small modular reactor, as part of the European Project McSAFER to investigate the performance of the helical-coiled heat exchanger and the cross-flow in the core. The objective of this paper is to validate the turbulent mixing model of the KIT in-house code TWOPORFLOW using data of the core cross-flow tests. The validation was carried out in two stages; first, simulations were performed using different mixing coefficient values for a uniform radial power profile at 235 kW. Second, the ring-shaped MOTEL test series were simulated. The results for the ring-shaped test series closely match the experimental data over the entire test. Overall, the results showed that the turbulent mixing model of TWOPORFLOW works well, being able to predict thermal-hydraulic parameters under natural circulation conditions close to those observed in the experiment.

KEYWORDS: TWOPORFLOW code, MOTEL experiment, small modular reactors, cross-flow, natural circulation, thermal-hydraulics, validation

I. Introduction

Over the last years, research devoted to Small Modular Reactors (SMRs) has gain importance around the world. In Europe, several projects related to the development of this technology have been funded.[1-4] The H2020 McSAFER Project combined safety-relevant thermal-hydraulic experiments with numerical simulations based on different approaches for safety evaluation of light water-cooled SMRs.[1]

The MOTEL (MOdular TEst Loop) facility has been constructed at LUT University in Lappeenranta, Finland.[5] The first facility configuration, used within McSAFER Project, resemble a typical integral PWR, like NuScale.[6] MOTEL's core configuration for cross-flow tests is divided in radial independent power regions, allowing large power gradients that lead to mixing among subchannels. The heater rods have a stepwise cosine-shaped axial power distribution.

The MOTEL instrumentation is limited to thermocouple measurements, so the goal in the experiments was to achieve measurable temperature differences in the radial directions of the core.

The MOTEL experimental program provided data for the validation of subchannel and CFD codes. In this work the ring-shaped sets of experiments were analyzed.

This paper is structured as follows: Section II provides a detailed description of the turbulent mixing model implemented in TWOPORFLOW. Section III presents the main characteristics of the MOTEL cross-flow test series, while Section IV depicts the TWOPORFLOW model for the cross-flow analysis. The validation activities and selected results are then discussed in Section V. Finally, Section VI provides the conclusions driven from this work.

II. Description of TWOPORFLOW Code Turbulent Mixing Model

The porous-media two-phase flow code TWOPORFLOW (TPF) is being developed at the Karlsruhe Institute of Technology (KIT) and recently it was applied to SMRs.[7,8] It has a six-equations formulation according to the two-fluid model. Mass, momentum and enthalpy conservation equations are written for both, the vapour and the liquid, phases in three-dimensions for rectangular meshes. Porosity is implemented by the Fractional Area-Volume Obstacle Representation (FAVOR) technique,[9] where the Darcy velocity is a velocity vector related to the subchannel surface porosity (φ) defined as follows:

$$\vec{w}_k = \begin{pmatrix} \varphi_x & V_{kx} \\ \varphi_y & V_{ky} \\ \varphi_z & V_{kz} \end{pmatrix}, \tag{1}$$

where, the subscripts x, y, z represent the Cartesian coordinates, and k becomes the fluid phase, liquid (l) or vapour (v). Equations containing this information are analogous to the equations for flow in porous media.

The turbulence model in TPF is based on the turbulent-viscosity hypothesis.[10] According to this hypothesis, the turbulent flow can be simulated as a pseudo-fluid having an effective viscosity (μ_k) that results from the sum of the molecular and turbulent viscosities of each phase,

$$\mu_k = \mu_{mol,k} + \mu_{tur,k}. \tag{2}$$

*Corresponding author, E-mail: alejandro.munoz@kit.edu

To calculate the turbulent viscosity ($\mu_{tur,k}$), an empirical mixing coefficient (β) determined experimentally, must be taken into account[11] according to the following expression:

$$\mu_{tur,k} = \beta \rho_k V_k D_h, \tag{3}$$

as characteristic length the hydraulic diameter (D_h) is used.

In strong upward dominated flow, vapour volume is transported in lateral direction. To model this effect, a void dispersion term is added to the vapour momentum equation for bubbly flow, calculated as follows:[12]

$$b_{dis} = 0.4\, \mu_{tur,l} \frac{V_l}{D_h}. \tag{4}$$

To include the turbulent flow effect in the energy conservation equation, the turbulent thermal conductivity (λ_{tur}) is calculated using the turbulent Prandtl number (Pr_{tur}), it is defined as:[13]

$$\lambda_{tur,k} = \frac{\mu_{tur,k} Cp_k}{Pr_{tur,k}}. \tag{5}$$

In TPF, a constant value of 0.9 for the turbulent Prandtl number is used for both, liquid and vapour phase.[14] Similar to the effective viscosity, the effective thermal conductivity (λ_k) is calculated by adding the turbulent thermal conductivity to the molecular heat conductivity:

$$\lambda_k = \lambda_{mol,k} + \lambda_{tur,k}. \tag{6}$$

Based on these assumptions, the conservation equations in TPF are following presented.

1. Mass Basic Equations

The mass conservation equations for the two phases are:

$$\frac{\partial(\alpha_l \rho_l \epsilon_V)}{\partial t} + \nabla \cdot (\alpha_l \vec{w}_l) = -\Gamma_I, \tag{7}$$

$$\frac{\partial(\alpha_v \rho_v \epsilon_V)}{\partial t} + \nabla \cdot (\alpha_v \vec{w}_v) = \Gamma_I, \tag{8}$$

where the sum of the fluid volume fraction is:

$$\alpha_l + \alpha_v = 1, \tag{9}$$

The source term Γ_I describes the rate of evaporation or condensation at the liquid-vapour interface. The heat exchange between phases is defined at the vapour interface as:

$$Q_{Iv} + \Gamma_I h_{v,sat} = Q_I, \tag{10}$$

and at the liquid interface as:

$$Q_{Il} - \Gamma_I h_{l,sat} = -Q_I. \tag{11}$$

The interfacial heat mass transfer rate is given by combining Eqs. (10) and (11):

$$\Gamma_I = -\left(\frac{Q_{Iv} + Q_{Il}}{h_{v,sat} - h_{l,sat}}\right). \tag{12}$$

2. Momentum Basic Equations

The momentum conservation equations are expressed in non-conservative form as follows:

$$\alpha_l \rho_l \frac{\partial \vec{V}_l}{\partial t} + \frac{\alpha_l \rho_l \vec{w}_l \nabla(\vec{V}_l)}{\epsilon_V} + \alpha_l \nabla(P) = -\vec{F}_{wl} + \vec{F}_I + \alpha_l \rho_l \vec{g} + \alpha_l \vec{D}_l, \tag{13}$$

$$\alpha_v \rho_v \frac{\partial \vec{V}_v}{\partial t} + \frac{\alpha_v \rho_v \vec{w}_v \nabla(\vec{V}_v)}{\epsilon_V} + \alpha_v \nabla(P) = -\vec{F}_{wv} - \vec{F}_I + \alpha_v \rho_v \vec{g} + \alpha_v \vec{D}_v - b_{dis} \nabla \alpha_v. \tag{14}$$

The viscosity diffusion terms are defined as:

$$\vec{D}_k = \frac{1}{\epsilon_V} \begin{pmatrix} \frac{\partial}{\partial x}\varphi_x \mu_k \frac{\partial V_x}{\partial x} + & \frac{\partial}{\partial y}\varphi_y \mu_k \frac{\partial V_x}{\partial y} + & \frac{\partial}{\partial z}\varphi_z \mu_k \frac{\partial V_x}{\partial z} \\ \frac{\partial}{\partial x}\varphi_x \mu_k \frac{\partial V_y}{\partial x} + & \frac{\partial}{\partial y}\varphi_y \mu_k \frac{\partial V_y}{\partial y} + & \frac{\partial}{\partial z}\varphi_z \mu_k \frac{\partial V_y}{\partial z} \\ \frac{\partial}{\partial x}\varphi_x \mu_k \frac{\partial V_z}{\partial x} + & \frac{\partial}{\partial y}\varphi_y \mu_k \frac{\partial V_z}{\partial y} + & \frac{\partial}{\partial z}\varphi_z \mu_k \frac{\partial V_z}{\partial z} \end{pmatrix}. \tag{15}$$

3. Energy Basic Equations

For energy conservation, the enthalpy (h) for nearly incompressible fluid is used, neglecting the work terms the energy balance equations are written as follows:

$$\frac{\partial(\alpha_l \rho_l \epsilon_V \mathrm{h}_l)}{\partial t} + \nabla \cdot (\alpha_l \rho_l \mathrm{h}_l \vec{w}_l) - K_l = Q_{sl} - Q_I, \tag{16}$$

$$\frac{\partial(\alpha_v \rho_v \epsilon_V \mathrm{h}_v)}{\partial t} + \nabla \cdot (\alpha_v \rho_v \mathrm{h}_v \vec{w}_v) - K_v = Q_{sv} + Q_I, \tag{17}$$

where, Q_s is the heat exchange between structure and fluid and Q_I is the heat exchange between the phases i.e., liquid and vapor. The thermal diffusion term (K_k) for liquid and vapor is given by:

$$K_k = \frac{\partial}{\partial x}\lambda_k \alpha_k \varphi_x \frac{\partial}{\partial x} T_k + \frac{\partial}{\partial y}\lambda_k \alpha_k \varphi_y \frac{\partial}{\partial y} T_k + \frac{\partial}{\partial z}\lambda_k \alpha_k \varphi_z \frac{\partial}{\partial z} T_k. \tag{18}$$

III. Description of the MOTEL's Cross-flow Experiment

1. MOTEL Core and Instrumentation

MOTEL's core is arranged in a rectangular grid, where 132 electrically heater rods, 145 dummy rods and 16 measurement rods are placed as presented in **Fig. 1**. The cladding material of all the rod types is stainless-steel (AISI316), while the geometrical dimensions are shown in **Table 1**. The maximum heating power of one rod is 7.5 kW, its axial power profile follows a stepwise cosine-shape (see **Fig. 2**), approximating the power distribution of a real nuclear power plant core. Each axial power sector is 0.366 m long.

Regarding the measurement positions, each measurement rod has 5 thermocouples (TC) axially distributed from bottom to top as presented in Fig. 2. These rods are radially distributed across the core, covering the 12 separately adjustable power regions, see **Fig. 3**.

The thermocouple measurement uncertainty is ±2 °C.[15] The mass flow is measured with ultrasonic flow meters.

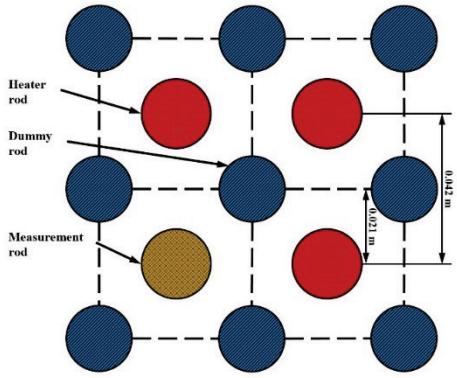

Fig. 1 MOTEL rectangular grid distribution

Table 1 MOTEL rods geometrical dimensions

Parameter	Value
Heater rod outer diameter	0.01905 m
Measurement rod outer diameter	0.01905 m
Dummy rod outer diameter	0.018 m
Cladding thickness	0.0007 m
Heater rod length	1.83 m

2. Ring-shaped Core Power Distribution Test Series

The cross-flow experimental test was performed using the ring-shaped radial power distributions. During the experiment, the pressure of the primary loop was kept constant at 2 MPa. The mass flow rate through the core oscillated between 4 and 11 kg/s. In total, five different power steps were tested. **Table 2** displays the power of each rod of the corresponding power sector.

Table 2 Power per heater rod in each power sector for the ring-shaped test series

	Power (kW)				
Sector	Step 1	Step 2	Step 3	Step 4	Step 5
S1	1.09	7.48	1.80	7.49	3.95
S2	1.09	0.00	1.80	0.70	2.33
S3	1.09	0.00	1.80	0.71	0.71
S4	1.09	0.00	1.80	0.70	2.33
S5	1.08	0.00	1.79	0.70	0.69
S6	1.09	0.00	1.80	0.71	0.71
S7	1.11	0.00	1.81	0.71	2.34
S8	1.10	7.48	1.80	7.51	3.96
S9	1.10	0.00	1.81	0.71	0.72
S10	1.09	0.00	1.79	0.71	0.72
S11	1.09	0.00	1.79	0.70	2.34
S12	1.09	0.00	1.80	0.70	0.72

The sequential power steps of the experiment were run as following:

1) 0 s - 1800 s, uniform profile at 150 kW.
2) 1800 s - 5400 s, first ring-shaped profile, two-rings.
3) 5400 s - 7200 s, uniform profile at 235 kW.
4) 7200 s - 10800 s, second ring-shaped profile, two-rings.
5) 10800 s - 14400 s, third ring-shaped profile, three-rings.

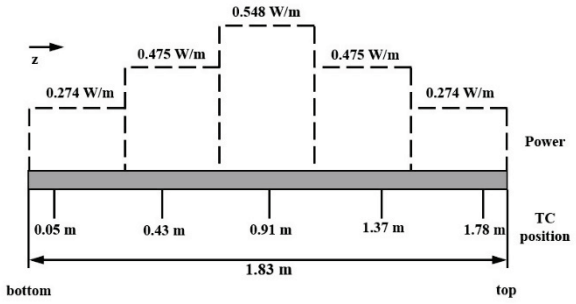

Fig. 2 Heater rod axial power profile and thermocouple locations

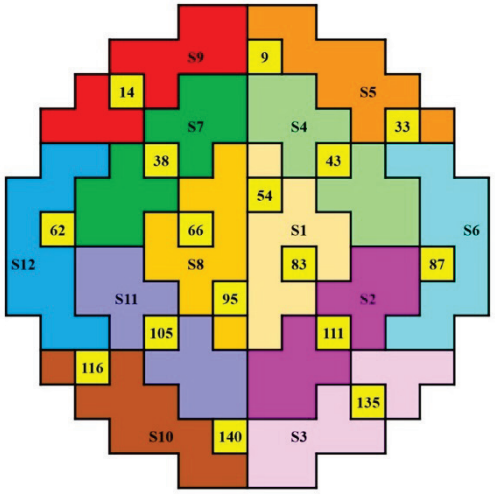

Fig. 3 Radial distribution of the measurement rods and independent radial power sectors

IV. Description of the TWOPORFLOW Model

A model of the MOTEL core was developed for TPF based on the experimental data previously presented given by LUT University.[15] Key TPF thermal-hydraulic parameters derived from the experimental data are presented in **Table 3**. The hydraulic diameter was calculated with the following formula:

$$D_H = \frac{1}{d+q}\left[\frac{4p^2}{\pi} - (d^2 + q^2)\right] \tag{19}$$

where, d is the dummy rod outer diameter, q is the heater/measurement rod outer diameter, and p is the subchannel side length. The X and Y porosities is calculated with the average outer diameter from the dummy and heater/measurement rods. The Z porosity is calculated with the sum of the dummy and heater/measurement rods.

Each one of the 132 heater rods and 16 measurement rods are represented by a rod centered subchannel, where the proportional part of the surrounding dummy rods is smeared over the subchannel (see **Fig. 4**). The core is represented by a 14×14 radial mesh grid with 25 axial levels. Each mesh cell has the dimensions of 42×42×73.2 mm. The temperature measurements are taken from the cell that holds the corresponding thermocouple position. The IAPWS-97 water properties were used, while stainless-steel 316 TPF internal correlations were used for heater and measurement rods.

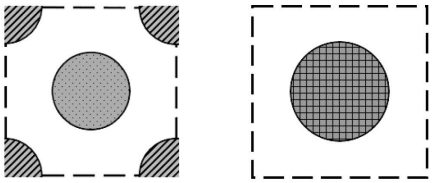

Fig. 4 Single MOTEL subchannel (left) and single representative rod centered subchannel in TPF (right)

Table 3 MOTEL geometrical parameters for TPF

Parameter	Value
Rod outer diameter	0.01905 m
Subchannel side length	0.042 m
Hydraulic diameter	0.04208 m
X, Y porosities	0.555
Z porosity	0.388

V. TWOPORFLOW Code Validation

1. Validation of the TWOPORFLOW Turbulent Mixing Model

The first validation stage of TPF is to study the impact of the turbulent mixing model and the respective mixing coefficient used in TPF. The selected MOTEL case was the 235 kW uniform radial power distribution (step 3 of Table 2). The coolant temperature measured by thermocouples at 5 axial locations of radial positions 9 and 54 (see Figs. 2 and 3) is compared with the ones predicted by TPF considering different turbulent mixing coefficients. The boundary conditions for these calculations are the following: mass flow rate of 8.5 kg/s, inlet coolant temperature of 159 °C and core outlet pressure of 2 MPa.

(1) Discussion of Results

In **Fig. 5**, it is shown the Root Mean Square Error (RMSE):

$$RMSE = \sqrt{\frac{\sum_{i=1}^{N}(EXP_i - TPF_i)^2}{N}} \quad (20)$$

for the temperature measurements at the radial locations 9 and 54 using different mixing coefficient values, from 0.0 to 0.4. Here, it can be seen that the error is significantly reduced moving from β=0.0 to β=0.05, while no significant improvement was observed using bigger mixing coefficient values. In **Table 4**, a comparison is presented between the temperature data measured by five axial thermocouples at locations 9 and 54 and the temperatures predicted by TPF using two different mixing coefficients.

For the uniform power profile, the deviations of the predicted coolant temperature at positions 9 and 54, and respective axial location from the measured data decrease considerably when the mixing is taken into account by TPF compared to the predictions without mixing. More specifically, the comparison of the TPF-predictions for the two upper thermocouples (1.37 and 1.78 m) with the measured temperatures is in very good agreement i.e., with deviations of around 1% compared to deviations of up to 3.5% when no mixing is considered.

If mixing is not taken into account in the TPF-simulations, the temperature predicted at the upper part decreases. This tendency is not observed in the experimental data. Conversely, when the turbulent mixing is taken into account the temperature increases similar to the measured one as expected. Based on these good results, a mixing coefficient value of β=0.05 is used for all cross-flow tests simulations in this work.

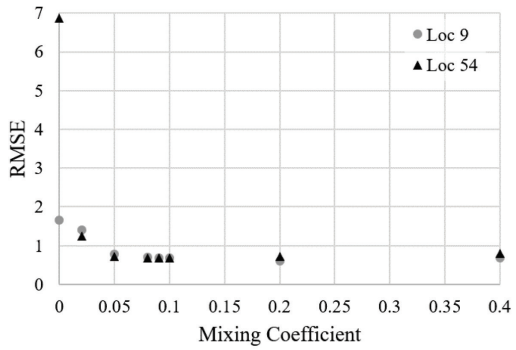

Fig. 5 Error comparison for different mixing coefficients

Table 4 Comparison between experiment (EXP) and simulation (TPF) with and without mixing model

		Temperature (°C) (Diff) (°C)		
Location	Height (m)	EXP	$\beta = 0.0$	$\beta = 0.05$
9	0.05	159.7	159.0	159.1
		(-)	(0.7)	(0.6)
	0.43	160.0	159.1	159.8
		(-)	(0.9)	(0.2)
	0.91	162.1	161.9	161.8
		(-)	(0.2)	(0.3)
	1.37	163.9	162.0	163.7
		(-)	(1.9)	(0.2)
	1.78	164.8	161.8	165.0
		(-)	(3.0)	(-0.2)
54	0.05	159.7	159.0	159.1
		(-)	(0.7)	(0.6)
	0.43	159.6	159.2	159.8
		(-)	(0.4)	(-0.2)
	0.91	162.0	162.0	161.8
		(-)	(0.0)	(0.2)
	1.37	163.8	160.4	163.6
		(-)	(3.4)	(0.2)
	1.78	165.0	159.1	165.0
		(-)	(5.9)	(0.0)

2. Validation of TWOPORFLOW using Data of the MOTEL Ring-shaped Power Distribution Test Series

The second validation stage of TPF was done simulating the MOTEL cross-flow test series. The boundary conditions such as power, mass flow rate and coolant temperature at the core inlets needed for the simulations were computed from the experimental measurements.[16] The experimental conditions (EXP) and the average (AVG) values used in the TPF simulation are shown in **Figs. 6** to **8**. The outlet pressure was kept constant at 2 MPa during the whole simulation. The radial power profiles are set as presented in Table 2.

(1) Discussion of the Comparison between Predictions and Experimental Data

For the evaluation of the TPF's prediction capability the data of the cross-flow test series with ring-shaped power profiles measured in the following three locations were selected:

- Location 9 holds a measurement rod consistently situated in a "cold" region, meaning no power or low power.
- Location 38, holds a measurement rod that is always at the "boundary" between a high power and a low power zone.
- Location 54 holds a measurement rod that always is in a "hot" region, i.e., with high power.

Figures 9 to **11** shows the coolant temperature comparison during the test series, between experimental data and TPF predictions at the three radial locations and two axial elevations. As it was previously mentioned, at the bottom of the core, the radial power gradient is low. Therefore, all the regions at the core inlet approximately the same coolant temperature, see **Fig. 12**. The comparison of the experimental data and simulation results at this elevation indicates a difference between them below 1 °C for the whole duration of the experiment. At the top of the core, cross-flow is observed for the three ring-shaped power profiles in both the experimental data and simulation results, see **Fig. 13**.

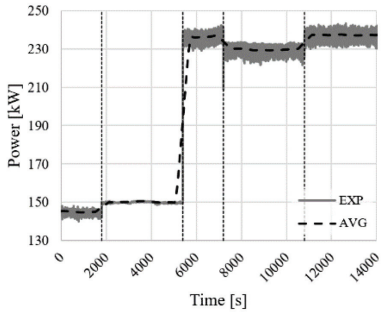

Fig. 6 Power transient boundary condition

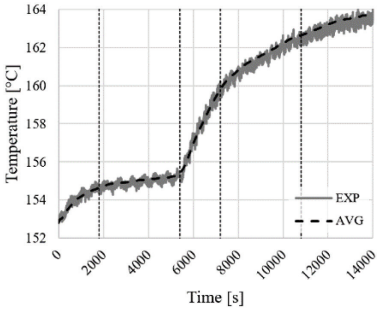

Fig. 7 Inlet temperature transient boundary condition

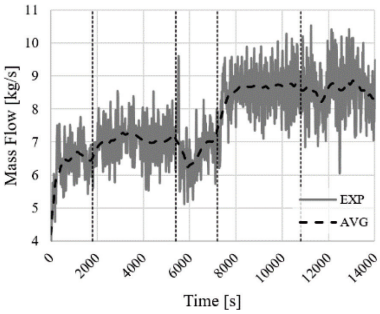

Fig. 8 Mass flow rate transient boundary condition

A comparison of the coolant temperature predicted by TPF for the upper elevation of location 9 (cold region) with the measured data shows a very good agreement along the test duration with a small underprediction for the steps 4 and 5. Similar comparison of the predictions and data for the Location 38 (boundary) for the upper elevation gives excellent agreement with a small overprediction only for the step 2, which is inside the measurement error of ±2 °C. Finally, the comparison of the TPF predictions at the Location 54 (hot) upper elevation with the measured coolant temperature, shows very similar trends of predictions and data which are in a good agreement with an overprediction in the steps 2, 4 and 5 that lies within the measurement error of ±2 °C.

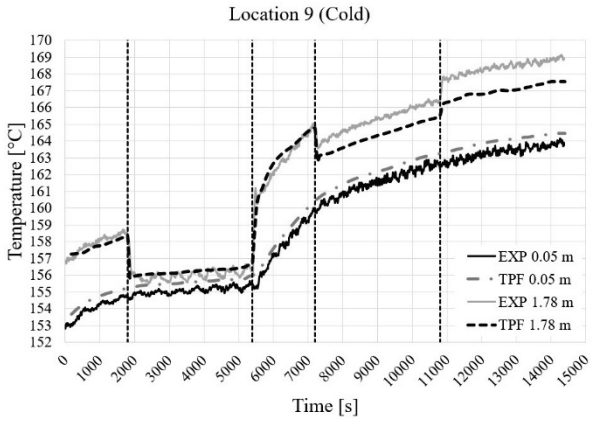

Fig. 9 Coolant temperature comparison at location 9

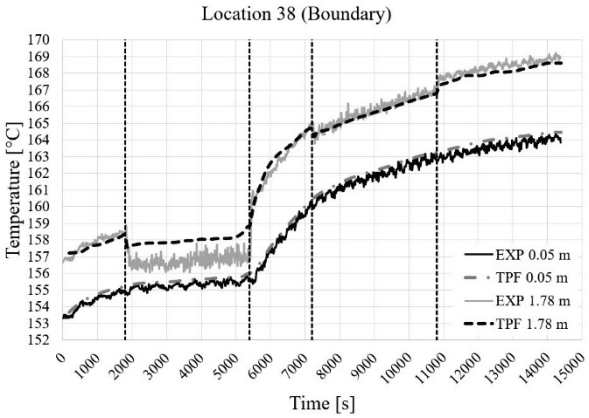

Fig. 10 Coolant temperature comparison at location 38

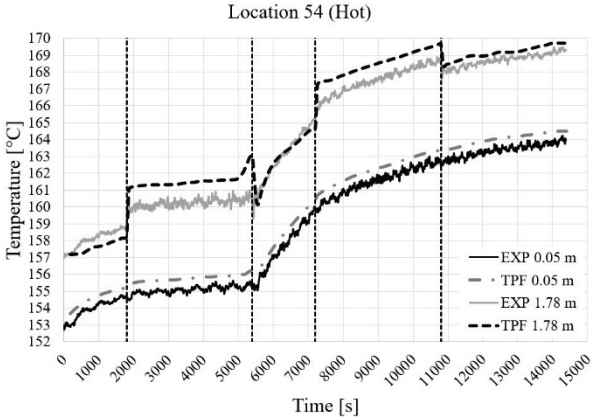

Fig. 11 Coolant temperature comparison at location 54

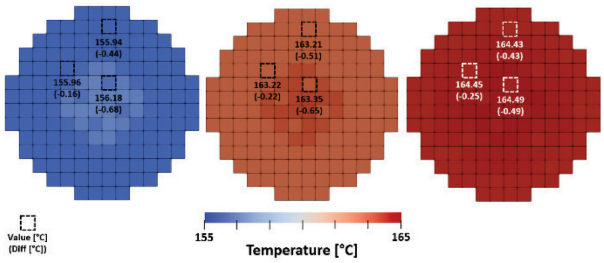

Fig. 12 Inlet radial temperature distribution for steps 2, 4, and 5

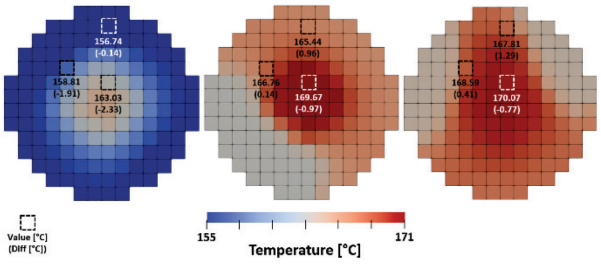

Fig. 13 Outlet radial temperature distribution for steps 2, 4, and 5

In general, it can be stated that the TPF-predictions for the ring-shaped profiles are qualitatively and quantitatively in good agreement to the measured temperature. Lastly, it can be observed that the differences of TPF predictions compared to the experimental data are very low for the steps 1 and 3 characterized by a uniform radial power distribution.

VI. Conclusions

This work presents the validation of TPF regarding turbulent mixing under natural circulation conditions using data from the MOTEL cross-flow test series. In the first validation stage, TPF demonstrates improved results for the uniform power profile when turbulent mixing is considered. A mixing coefficient of 0.05 has proven to be suitable for a reasonably good prediction of the measured data. In the second validation stage, the MOTEL's ring-shaped test series were analyzed, cross-flow was observed in the calculations. Although the coolant temperature gradient at the upper part of the core is larger than the experimentally observed, indicating less mixing. Nevertheless, the calculated coolant temperatures overall exhibit very good agreement with the reference data. These results lead to the conclusion that the turbulent mixing model implemented in TPF performs well and the code is capable of simulating natural circulation conditions at low mass flow rates.

Acknowledgment

The authors thank the HGF Program NUSAFE and the BMBF Innovation Pool SMR Initiative for financial support as well as partly for to the Horizon 2020 research and innovation program of the EU under the grant agreement number 945063. The authors appreciate the support of the experimental team of the MOTEL facility of the LUT University of Finland, as well as the support of TRACTEBEL given for the time dependent boundary conditions.

References

1) V.-H. Sanchez-Espinoza, S. Gabriel, H. Suikkanen, J. Telkkä, V. Valtavirta, M. Bencik, S. Kliem, C. Queral, A. Farda, F. Abéguilé, P. Smith, P. Uffelen, L. Ammirabile, M. Seidl, C. Schneidesch, D. Grishchenko, H. Lestani, "The H2020 McSAFER Project: Main Goals, Technical Work Program, and Status," *Energies*, (2021).
2) Lansou, et. al., "ELSMOR – towards European Lisensing of Small Modullar Reactors: Methodology recommendentions for light-water small modullar reactors safety assessment," *Open Reaserch Europe*, (2023).
3) PASTELS: passive systems simulating the thermal-hydraulic with experimental studies, www.pastels-h2020.eu
4) F. Mascari, "Safety Analysis of SMR with Passive Mitigation strategies – Severe Accident (SASPAM-SA) Horizon Euratom Project", *ETSON NEWS*, Sept. (2022). www.etson.eu/node/290
5) J. Hyvärinen, J. Telkkä, O.-P. Kauppinen, H. Purhonen, "MOTEL – modular design and physical scaling principles of the next generation thermal test facility at LUT," *Proc. of NURETH-17*, Sept. 3-8, 2017, Xi'an, China (2017).
6) NuScale, *NuScale Standard Plant Design Certification Application Chapter Four: Reactor*, NuScale Power LLC, (2020).
7) V. Jauregui-Chavez, U. Imke, V.-H. Sanchez-Espinoza, "TWOPORFLOW: A two-phase flow porous media code, main features and validation with BWR-relevant bundle experiments," *Nuclear Engineering and Design*, (2018).
8) A. Campos-Munoz, V.-H. Sanchez-Espinoza, E. Redondo, C. Queral, "Verification of the Coupled Code PARCS/TWOPORFLOW with Rod Ejection Accident Calculations for Small Modular Reactors," *Nuclear Science and Engineering*, (2024). doi: 10.1080/00295639.2024.2357953
9) C. W. Hirt, "Volume-fraction techniques: powerful tools for wind engineering," *Journal of Wind Engineering and Industrial Aerodynamics*, **46-47**, 327-338 (1993); doi: 10.1016/0167-6105(93)90298-3.
10) J. Boussinesq, "Essai sur la théorie des eaux courantes," *Mémoires présentés par divers savants à l'Académie des Sciences*, (1877).
11) F. Castellana, W. Adams, J. Casterline, "Single-phase subchannel mixing in a simulated nuclear fuel assembly," Nuclear Engineering and Design. **26**[2], 242–249 (1974). doi: 10.1016/0029-5493(74)90059-4.
12) M. Valette, "Analysis of subchannel and rod bundle PSBT experiments with CATHARE 3," *Science and Technology of Nuclear Installations*, (2012). doi: 10.1155/2012/123426.
13) S. Kim, S. Jang, "Effects of the Darcy number, the Prandtl number, and the Reynolds number on local thermal non-equilibrium," *International Journal of Heat and Mass Transfer*, **45**[19] (2002). doi: 10.1016/S0017-9310(02)00109-6.
14) A. Malhorta, S. Kang. "Turbulent Prandtl number in circular pipes," *International Journal of Heat and Mass Transfer*, **27** [11] (1984). doi: https://doi.org/10.1016/0017-9310(84)90203-5
15) K. Tielinen, J. Telkkä, E. Kotro, V. Kouhia, H. Suikkanen, *D2.4: Description of the MOTEL facility and instrumentation*, McSAFER (2021).
16) J. Telkkä, H. Suikkanen, A. Räsänen, E. Kotro, *D2.6: Results of the MOTEL transversal flow experiments*, McSAFER (2022)